ASIAN JOURNAL OF CIVIL ENGINEERING (BUILDING AND HOUSING) VOL. 9, NO. 3 (2008)
PAGES 261-290

NEAR-SOURCE ATTENUATION RELATIONSHIP FOR THE GEOMETRIC MEAN HORIZONTAL COMPONENT OF PEAK GROUND ACCELERATION AND ACCELERATION RESPONSE SPECTRA

H. Aghabarati* and M. Tehranizadeh
Department of Civil and Environmental Engineering, Amirkabir University of Technology, Hafez Avenue, Tehran, Iran

Abstract

Empirical ground motion models for the average horizontal component of peak ground motion and acceleration response spectra from shallow crustal earthquakes are derived using near-source database. These models were derived using a worldwide dataset consisted of corrected and processed accelerograms of 646 strong-motion records recorded with 60 (km) of the surface projection of earthquakes between M_w 5.2 and 7.8. Model is function of earthquake mechanism, distance from source to site, local average shear wave velocity, nonlinear soil response, sediment depth, depth-to-top of rupture, hanging wall effects and faulting mechanism. Non-linear site effects are constrained by equivalent linear models. An important additional source parameter, depth to the top is also included. The hanging wall effect is included with an improved model that varies smoothly as a function of the source properties, such as magnitude, dip, distance, depth, and the site location.

Keywords: Empirical ground motion; shallow crustal earthquake; near-source; faulting mechanism; nonlinear soil response; sediment depth; depth-to-top; hanging wall

1. Introduction

A more critical part of seismic design of structures is development of design ground motions. Methods are commonly used to develop these ground motions include: seismic zoning maps, site specific deterministic analysis and site specific probabilistic seismic hazard analysis. All this methods requires strong ground attenuation relationships to estimates earthquake ground motions from parameters characterizing the earthquake source, the propagation path and geological condition. On the other hand, design ground motions are often controlled by hypothesized occurrence of a large earthquake on near by faults; therefore, it is important that the seismological model or attenuation relationship used to

*E-mail address of the corresponding author: aghabarati@aut.ac.ir (H. Aghabarati)

predict these design ground motions specifically address this requirement. In the two past decade sufficient strong motion records from close to large magnitude, earthquakes have become available to derive equations for estimating ground motions using only these records. In this study, empirical models for the attenuation of response spectral values for average horizontal component and acceleration response spectra applicable to shallow crustal events in active tectonic regions are developed.

In 1994, Campbell and Bozorgnia developed a comprehensive near-source ground motion relation for horizontal peak ground acceleration (PGA) in response to the 1992 Petrolia and Landers, California, earthquakes [1]. Campbell [2] merged this 1994 relation with previous ground motion relations that he had developed for peak ground velocity (PGV), pseudo acceleration response spectra (PSA), and the vertical component of ground motion to use in engineering [2]. In 2003, Campbell and Bozorgnia developed a new near-source ground motion for vertical and horizontal PGA and PSA, that their relation had some near-source effects such as hanging wall effect [3]. Ambraseys and Douglas also developed alternatively ground motion for PGA in near-fault regions [4]. Many of these relations had different functional forms that led to a somewhat awkward and complicated set of ground motion relations. In order to remedy this situation, we presented a new analysis using a consistent set of strong motion recordings and functional forms to develop a mutually consistent set of near-source ground motion relations for the average horizontal components of PGA and 5% damped PSA. We decide to incorporate some important earthquakes occurred currently to our database. We also took this opportunity to develop PGA database with selected recordings from the 1994 Northridge, California, and 1995 Kobe, Japan, 1999 Kocaeli, Turkey, 1999 Hector mine, California, 2002 Denali, Alaska earthquakes and improve PSA database with these recordings plus selected recordings from earthquakes since 1940. Another important aspect of the study was to gain a better understanding of the characteristics of the soil response and Basin effects. It is important to recognize that this study was intended to be a development of the ground motion relations derived previously, with the explicit purpose of providing engineers and seismologists with a mutually consistent set of near-source ground motion relations for use in seismic hazard analysis. As to this development, the study explicitly address such topics as sediment depth, hanging wall, depth-to-top of the rupture and the use of the 30 (m) velocity related to National Earthquake Hazard Reduction Program (NEHRP) site classes. However, the study refines some of the parameters previously used by other researches [1-4] and including these especial effects:

- hanging wall effects
- dividing events into three main categories (reverse (thrust), strike-slip and normal faulting)
- linear and nonlinear soil properties
- depth-to-top of the rupture effects

In the following section, we will first describe our strong ground motion database used in the analysis (Section 2). We will then move on to introduce the regression methodology used for development of attenuation relationship (Section 3). The ground motion model for average horizontal component of PGA and PSA will be presented in section 4. The model results are given in section 5 and finally comparison of the model results with the existing ground motion

relations that are widely used in engineering seismology can be found in section 6.

2. Strong Motion Data

We selected 646 strong motion records from near-source worldwide accelerograms recorded over the 63 year time period from 1940 to 2002. The database consist of mainshocks and aftershocks records from 54 crustal earthquakes following the free-field definition of Joyner and Boore [5] using the criteria: $M_W \geq 5.2$, $R_{rup} \leq 60(km)$ and $h \leq 15(km)$.

The database was expanded and Developed from that dataset used previously by Campbell and Bozorgnia [3], Ambraseys and Douglas [4], Abrahamson and Silva [6] and Sedigh et al. [7]. We expanded the database to include PGA and PSA values from six earthquakes that occurred from 1995 to 2002. All of the selected recordings come from instrument shelters or non-embedded buildings less than three stories high (less than seven stories high if located on firm rock). Records on dam abutments are included to enhance the database, even though there could be some interaction between the dam and the recording site. We excluded recordings in the basements of buildings of any size, in buildings over two stories high (over six stories high if located on firm rock), or on the toe or base of a dam because of the potential adverse effects of instrument embedment and soil-structure interaction [2-4]. The chosen records and their characterizes are listed in Table 1. The distribution of the records used with respect to their locations and earthquake mechanism is also given in Table 1. Although some authors have found evidence for differences in strong ground motions due to the tectonic environment, the limited number of records fulfilling our selection criteria meant that we could not investigate this effect [8]. However, all the records in our database came from shallow crustal earthquakes in active tectonic regions, except for three records from the 1976 Gazli, 1985 Nahanni and 2002 Denali earthquakes which are from a stable continental region and have been used in data set of previous researches [2, 3, 4, 6, 7, 9]. We excluded subduction interface earthquakes, since such events occur in an entirely different tectonic environment than the other shallow crustal earthquakes and it has not been clearly shown that their near-source ground motion is similar to that of shallow crustal earthquakes.

Figure 1 shows the distribution of the data with magnitude and distance. As can be seen from Figure 1 the records are well distributed in magnitude and distance, and consequently the equations obtained, based on this set of data are well constrained and representative of the entire data space: $0 \leq R_{nip} \leq 60(km)$ and $5.2 \leq M_W \leq 7.9$. The distribution is reasonably uniform and suggests that there was no need to use special statistical procedures to decouple source and path effects in the regression analysis, at least over the M_W:6.0-7.5 magnitude range that is of greatest engineering interest. The strong motion parameters included corrected peak ground acceleration and 5% damped PSA at natural periods ranging from 0.01 to 10.0 sec. Because our interest is in shallow crustal earthquakes in seismically and tectonically active regions, we included only earthquakes with focal depths less than 15 (km) located in seismic regions believed to have source and near-source attenuation characteristics. Definition of the size of an earthquake uniformly is in terms of M_W and we defined the source to site distance in terms of $R_{rupture}$, defined as the shortest distance between the recording site and the surface projection of

rupture plane of earthquakes. We restricted recording sites to $R_{rup}\leq 60(km)$ to avoid complications related to the arrival of multiple reflections from the lower crust that was observed during the some earthquakes. This distance range would include most of strong ground motion investigation of engineering seismology. Sediment depth has been found to be strongly correlated with the amplitude of long-period spectral acceleration [2, 10, 11]. Joyner [12] found that the amplification of long-period ground motion predicted from sediment depth from the ground motion relation was reasonably consistent with the predicted amplification from surface wave generation at the edge of the Los Angeles Basin. The SCEC 3-D basin response-modeling group simulated the long period ground motions in the Los Angeles region from nine different fault sources [13,14]. In our model, we used a depth to $V_{S30}=1500(m/s)$ since it has a much better chance of being obtained for engineering projects. We classified the faulting mechanism of an earthquake into one of three main categories defined as strike slip, normal and reverse.There is a lack of near-field recordings of earthquakes with normal mechanisms in the dataset used and there are no records from normal earthquakes with $M_W>6.9$ because of fault segmentation. Based on a comparison with the Boore et al. [15] and Spudich et al. [8], they concluded that earthquakes with normal faulting mechanisms in extensional stress environments have lower median predicted ground motion at some periods and distances than earthquakes that occur in compressional stress environments.

Table 1. Database of strong-motion recordings

Number of Records	Mechanism Based on Rake Angle	Earthquake Magnitude (M_W)	Year	Location	Earthquake Name
1	Strike Slip	6.95	1940	Western United States (WUS)	Imperial Valley
1	Thrust	7.36	1952	WUS	Kern County
4	Strike Slip	6.19	1966	WUS	Parkfield
1	Strike Slip	6.63	1968	WUS	Borrego Mtn
19	Thrust	6.61	1971	WUS	San Fernando
1	Strike Slip	7.68	1972	Alaska	Sitka
1	Strike Slip	6.24	1972	Nicaragua	Managua
1	Reverse oblique	7.21	1976	Turkey	Caldiran
1	Reverse	6.80	1976	USSR	Gazli
3	Thrust	6.50	1976	Italy	Friuli
4	Thrust	5.91	1976	Italy	Friuli Aftershock
3	Thrust	7.35	1978	Iran	Tabas
2	Thrust	5.92	1978	WUS	Santa Barbara
1	Thrust	7.54	1979	Alaska	St Elias
33	Strike Slip	6.53	1979	WUS	Imperial Valley
10	Strike Slip	5.74	1979	WUS	Coyote Lake
12	Normal	6.90	1980	Italy	Irpinia
9	Normal	6.20	1980	Italy	Irpinia Aftershock

Number of Records	Mechanism Based on Rake Angle	Earthquake Magnitude (M_W)	Year	Location	Earthquake Name
4	Strike Slip	6.33	1980	Mexico	Victoria, Mexico
3	Reverse oblique	6.06	1980	WUS	Mammoth Lakes
3	Strike Slip	5.69	1980	WUS	Mammoth Lakes Aftershock
1	Normal	6.60	1981	Greece	Corinth
6	Strike Slip	5.90	1981	WUS	Westmorland
46	Thrust	6.36	1983	WUS	Coalinga
26	Strike Slip	6.19	1984	WUS	Morgan Hill
5	Normal	5.80	1984	Italy	Lazio-Abruzzo
3	Thrust	6.76	1985	Canada	Nahanni
2	Reverse oblique	5.20	1985	Greece	Drama
11	Strike Slip	6.19	1986	WUS	Chalfant Valley
5	Strike Slip	5.77	1986	WUS	Chalfant Valley Aftershock
26	Reverse	6.06	1986	WUS	N. Palm Springs
2	Strike Slip	5.80	1986	WUS	San Salvador
1	Normal	6.60	1987	New Zealand	New Zealand
1	Strike Slip	6.22	1987	WUS	Superstition Hills
11	Strike Slip	6.54	1987	WUS	Superstition Hills Aftershock
107	Reverse	5.99	1987	WUS	Whittier Narrows
57	Reverse	6.93	1989	WUS	Loma Prieta
2	Strike Slip	7.37	1990	Iran	Manjil
2	Normal	6.10	1990	Greece	Griva
9	Thrust	5.61	1991	WUS	Sierra Madre
13	Strike Slip	7.28	1992	WUS	Landers
6	Thrust	7.01	1992	WUS	Cape Mendocino
1	Strike Slip	6.69	1992	Turkey	Erzican
3	Normal	5.65	1992	WUS	Little Skull Mtn
129	Thrust	6.69	1994	WUS	Northridge
1	Strike Slip	5.90	1994	WUS	Double Springs
1	Strike Slip	7.20	1995	WUS	Gulf of Aqaba
7	Strike Slip	6.90	1995	Japan	Kobe
3	Normal	6.40	1995	Turkey	Dinar
3	Normal	6.40	1995	Greece	Kozani
15	Strike Slip	7.51	1999	Turkey	Kocaeli
12	Strike Slip	7.14	1999	Turkey	Duzce
8	Strike Slip	7.13	1999	WUS	Hector Mine
4	Strike Slip	7.90	2002	Alaska	Denali

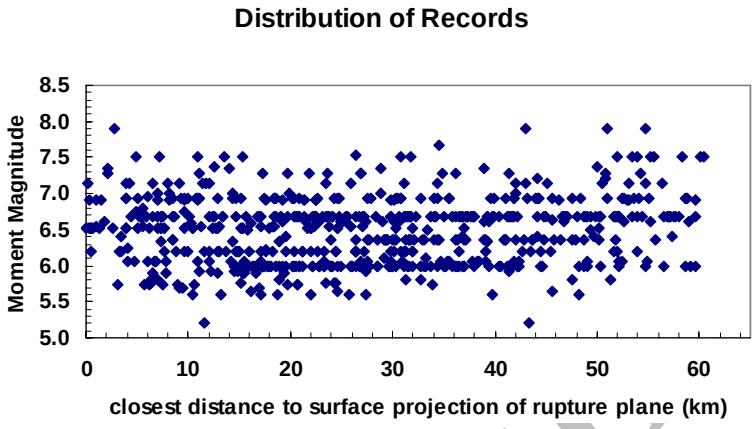

Figure 1. Distribution of all records in near-source dataset with respect to magnitude and distance

However, these authors also included strike-slip and normal earthquakes in their extensional database, which were also included in our study and in many other empirical studies using worldwide data. They also noted that by constraining their site parameter, they built in an inherent under prediction of their ground motion estimates on rock, which might have contributed, at least partially, to their conclusion. Therefore, consistent with past studies, we included a few earthquakes that Spudich et al. [8] would claim come from an extensional stress environment in our strike-slip and normal category. In previous studies, researchers classified local site conditions at each recording site into one of four categories defined as firm soil, very firm soil, soft rock, or firm rock. The geologic based site categories defined in this study can be approximately related to the average shear wave velocity in the top 30 (m) of the site, V_{S30}, based on statistical analyses of measured V_{S30} for similar geologic units reported by Wills and Silva [16] and Wills et al. [17] and by Park and Elrick [18]. A key change from previous models is that we are using V_{S30} rather than broad categories for the site classification. We used a slight modification of the site amplification given by Choi and Stewart [19].

3. Development Model of Attenuation Relations Based on Regression Methodology

We use a random effects model for the regression analysis. The random effects model is a maximum likelihood method that accounts for correlation in the data recorded by a single earthquake. For example if an earthquake has a higher than average stress drop, then the ground motion at all sites from this event are expected to be higher than average. In standard fixed effects regression, the model can be written as,

$$\ln y_i = f(M_i, R_i) + \varepsilon_i \qquad (1)$$

Where $y_{i,j}$ is the ground motion, M_i is the magnitude and R_i is the distance for the i data point. The ε_i term is assumed to be normally distributed with mean zero. The standard error of the ε_i values given the standard error of the model. In contrast, the random effects model can be written as

$$\ln y_{i,j} = f\left(M_i, R_{i,j}\right) + \eta_i + \varepsilon_{i,j} \tag{2}$$

Where $y_{i,j}$ is the ground motion for the j th recording from the i th earthquake, M_i is magnitude of the i th earthquake and $R_{i,j}$ is the distance for the j th recording from i th earthquake. The two stochastic terms in the model ε_{ij} and η_i are assumed to be normally distributed with mean zero. The random effects model uses the maximum likelihood method to partition the residual for each recording into ε_{ij} and η_i terms. This algorithm uses an iterative approach to finding the maximum likelihood solution. For a normally distributed data, the likelihood is given by

$$\begin{aligned}\ln L = &-\frac{1}{2}N\ln(2\pi) - \frac{1}{2}(N-M)\ln\sigma^2 - \frac{1}{2}\sum_{i=1}^{M}\ln\left(\sigma^2 + n_i\tau^2\right) \\ &-\frac{1}{2\sigma^2}\sum_{i=1}^{M}\sum_{j=1}^{n_i}\left(y_{ij} - \overline{Y}_i\right)^2 - \frac{1}{2}\sum_{i=1}^{M}\frac{n_i\left(\overline{Y}_i - \overline{\mu}_i\right)}{\sigma^2 + n_i\tau^2}\end{aligned} \tag{3}$$

$$\overline{Y}_i = \frac{1}{n_i}\sum_{j=1}^{n_i} y_{ij} \tag{4}$$

$$\overline{\mu}_i = \frac{1}{n_i}\sum_{j=1}^{n_i} \mu_{ij} \tag{5}$$

Where N is the number of data records, n_i is the number on records in event i th, M is the number of events and $\mu_{i,j}$ is the predicted value: $\mu_{i,j}=f(M_i, r_{i,j}, c)$. There are no analytical solutions for maximizing the likelihood in equation (3), so it must be maximized numerically. For given model parameter values c, variances σ^2 and τ^2, the maximum likelihood solution for the random effects, η_i, is

$$\eta_i = \frac{\tau^2\sum_{j=1}^{n_i} y_{ij} - \mu_{ij}}{n_i\tau^2 + \sigma^2} \tag{6}$$

Eq. (6) shows how the maximum likelihood method partitions the error term into inter-event and intra-event terms. Using this alternative approach, the algorithm for estimating σ^2, τ^2, and c is as follows:

1. Estimate the model parameter values, c, using a fixed effects (Eq. (1)) regression procedure.
2. Given c, estimate σ^2 and τ^2 by maximizing the likelihood given in Eq. (3).

3. Given c, σ^2 and τ^2, estimate η_i by Eq. (6).
4. Given η_i, estimate new c using a fixed effects (Eq. (1)) regression procedure for ($\ln y_{ij} - \eta_i$).
5. Repeat steps 2, 3, and 4 until the likelihood in step 2 is maximized.

If the standard deviations are not constant (e.g. the data are heteroscedastic), then Eq. (6) is modified to use the mean value of σ and τ for each event.

There are two parts of the standard error for the model: an inter-event term τ which is the standard error of the η_i and intra-event term σ which is the standard error of the $\varepsilon_{i,j}$. The total standard error of the model is

$$\sigma_{total} = \sqrt{\sigma^2 + \tau^2} \tag{7}$$

Several recent attenuation studies have found that the standard error is dependent on the magnitude of the earthquake. In this study both inter-event τ and intra event σ standard errors are allowed to be magnitude dependent and are modeled as linear magnitude dependence.

4. Regression Model of Ground Relations

The equation we selected to represent the ground motion relations for both the average horizontal components of PGA and PSA is given by

$$\begin{aligned} \ln y = {} & c_1 + f_1(M_W) + f_2(M_W) f_3(R) + f_4(F) + FR.f_5(Z_{FR}) + FS.f_6(Z_{FR}) \\ & + f_7(HW, R_{JB}, M_W, DIP) + f_8(V_{S30}, V_{lin}, PGA_{non-lin}, PGA_{rock}) + f_9(V_{S30}, Z_{1.5}) \end{aligned} \tag{8}$$

4.1 Scaling of magnitude

The magnitude scaling characteristics $f_1(M_w)$ and $f_2(M_W)$ are given by (M_W is moment magnitude)

for $M_W \le c_0$

$$\begin{aligned} f_1(M_W) &= c_3(M_W - c_0) + c_8(T)(8.5 - M_W)^n \\ f_2(M_W) &= c_2(T) + c_4(M_W - c_0) \end{aligned} \tag{9(a)}$$

for $M_W > c_0$

$$\begin{aligned} f_1(M_W) &= c_5(M_W - c_0) + c_8(T)(8.5 - M_W)^n \\ f_2(M_W) &= c_2(T) + c_6(M_W - c_0) \end{aligned} \tag{9(b)}$$

The magnitude dependent slope accommodates the saturation of high frequency ground motion at short distances. For long periods linear magnitude dependence is not adequate. Most recent studies have found that higher order terms are needed. Boore et al. [15] includes a quadratic term, Idriss [20] includes an exponential magnitude term, Campbell includes a hyperbolic arctangent term and Sedigh et al. [7] and Abrahamson and Silva [6] include a higher order polynomial term. These different models give similar models when fit to the

same data. We have adopted the polynomial function order two ($n = 2.0$) for magnitude term in long periods.

4.2 Scaling of distance

The distance scaling characteristics are given by

$$f_3(R) = \ln \sqrt{R_{rup}{}^2 + c_7(T)^2} \tag{10}$$

Several different distance definitions have been used for developing attenuation relations. We have used the closest distance to the rupture plane R_{nip} in our model. For the distance term inside the log, we have used the model similar to that used by Boore et al. [15]. In the Boore model, the $c_7(T)$ term can be inferred as a fictitious depth. We are using the rupture distance which can include depth for dipping faults and for fault that do not reach the surface, so the interpretation of $c_7(T)$ as a depth term is not clear. However, we have adopted this distance term because it yields a marginally better fit to the data at short distances. The $c_7(T)$ term is constrained to be monotonically varying with period; otherwise, there can be large changes in the spectral shape as the model is extrapolated to very short distances.

4.3 Style of faulting mechanism

Somerville and Pitarka [21] found that there is a difference in the ground motion for earthquakes with buried ruptures as compared to earthquakes with surface rupture. The buried ruptures lead to larger short period ground motions than the surface rupture earthquakes. Large reverse earthquakes tend to be buried ruptures more often than large strike-slip earthquakes so the effect of buried ruptures may have been partially incorporated in the faulting mechanism. The difference between ground motions from strike slip, reverse and normal has been become common in recent attenuation relations. The distinction between strike slip, reverse and normal events called the style of faulting mechanism. Most attenuation relations have considered a constant style of faulting mechanism that applied to all magnitude, distance and periods. In our study, we have used a period dependence to the style of faulting mechanism given by

$$f_4(F) = c_9(T)FR + c_{10}(T)FS + c_{11}(T)FN \tag{11}$$

4.4 Depth to top

For magnitudes less than 5.8, the magnitude dependence may have been due to depth-to-top effects. Small earthquakes have a larger average depth-to-top than larger magnitude earthquakes. In this evaluation, we consider the dependence on depth-to-top. The inter-event residuals from a preliminary regression are exhibit to be functions of rake and depth to the top of rupture. Its dependence is stronger to depth-to-top than the rake dependency. The reverse earthquakes exhibit a stronger scaling with depth in the top 2-10 (km). There is a correlation between the magnitude and the depth-to-top of rupture. The correlation for $5 \leq M_W \leq 6$ is much weaker. The smaller earthquakes tend to have a larger depth to top than the larger earthquakes. As a result, some of the depth dependence seen in the inter-event

residuals can be explained by magnitude scaling. We used earthquakes from this limited magnitude range to check the depth dependence. The depth-to-top of rupture dependence of the PGA inter-event residual for $5 \leq M_W \leq 6$ shows that for this limited magnitude range, there remains a trend of increasing inter-event residual with Z_{top}, although this trend is not just of the correlation of depth-to-top of rupture and magnitude. A linear model was selected for the depth-to-top dependence including different scaling of the depth-to-top for reverse and strike-slip earthquakes (no independence was found for normal faulting). This model will result in a larger apparent style of faulting mechanism for smaller magnitudes, consistent with the trend of a magnitude dependent style of faulting mechanism in the model.

$$f_5(Z_{FR}) = \begin{cases} 0 & \\ c_{12}(T)\left(\dfrac{Z_{top}-2}{3}\right) & Z_{top} \leq 2\,km \\ c_{12}(T) & 2 < Z_{top} \leq 5 \\ c_{12}(T)\left(1-\dfrac{Z_{top}-10}{5}\right) & 5 < Z_{top} \leq 10 \\ 0 & 10 < Z_{top} \end{cases} \quad (12)$$

$$f_6(Z_{FS}) = \begin{cases} c_{13}(T)\left(\dfrac{Z_{top}}{2}\right) & 0 < Z_{top} \leq 2\,km \\ c_{13}(T) & 2 < Z_{top} \leq 4 \\ c_{13}(T)\left(1-\dfrac{Z_{top}-4}{2}\right) & 4 < Z_{top} \leq 6 \\ 0 & 6 < Z_{top} \end{cases} \quad (13)$$

Where Z_{top} is the depth-to-top of the rupture in km.

4.5 Hanging wall effect

Strong hanging wall (HW) effects on short period ground motion was recognized in the 1994 Northridge earthquakes (Abrahamson and Somerville, [22]). The hanging wall effect is considered primarily a geometric effect that results from distant definition. The empirical residuals and the 1-D rock simulations both show strong HW effects. For site located over the HW, the short period ground motion was larger than for sites located at the same rupture distance on the foot wall (FW). The use of Joyner and Boore distance measure implicitly accounts for some aspects of the HW effects. Since the model is based on the rupture distance, we have included a specific Hanging Wall effects.

We use the 1-D rock simulations to evaluate the attenuation of the HW effect off the up-dip and down-dip ends of the rupture. The simulated ground motions for several reverse cases were fit to a simple form, similar to the approach followed by Collins et al. [23] but with the following changes. The data on the HW side, within the bounds of the rupture were excluded to produce a non-HW model for comparison with the HW sites, each magnitude had its own slope with distance and each event had it own constant. The residuals were then computed for sites on the FW and HW sides of the rupture, within the bounds of the rupture. Although the HW effects, affect some of the stations in our data set, this is important for engineering applications.

To include a HW term without the shortcomings described above requires a complicated model. Based on the analysis of the residuals discussed above, the functional form for the HW effect was developed that includes several tapers on the HW effect: tapers on distance, magnitude, and dip. First, there is a taper of the HW effect as the site moves away from being directly over the rupture. The Joyner and Boore distance is a measure of how far the site is from being over the HW, so we use the R_{JB} distance for the reduction.

$$g_1(R_{JB}) = \begin{cases} 1 - R_{JB}/45 & 0 \le R_{JB} < 15 \\ \frac{2}{3}(2 - R_{JB}/15) & 15 \le R_{JB} < 30 \\ 0 & 30 \le R_{JB} \end{cases} \tag{14}$$

The scaling of the HW effects with magnitude is stronger than the scaling with dip. The HW effect decreases near zero at about $M_W = 6.0$ and is approximately constant for $M_W \ge 6.5$. Therefore, we included a reduction on the magnitude in this range.

$$g_2(M_W) = \begin{cases} 0 & M_W < 6.0 \\ 2(M_W - 6) & 6.0 \le M_W < 6.5 \\ 1 & 6.5 \le M_W \end{cases} \tag{15}$$

Finally, we included a decrease on the dip. There is not a strong dependence on dip in the residuals, but the model should transition to no HW effect as the dip increases to 90. We applied a reduction from 70 degrees to 90 degrees from full effect to zero effect.

$$g_3(Dip) = \begin{cases} 1 - (Dip - 70)/20 & Dip \ge 70 \\ 1 & Dip < 70 \end{cases} \tag{16}$$

It is recognized that this HW model is complicated, but we think that its complexity is justified so that the model will vary smoothly based on the source properties and on site location. For the regression analysis, only a single HW parameter $c_{14}(T)$ is estimated. The other parameters in the three decreased functions are all held fixed.

$$f_7(HW, R_{JB}, M_W, DIP) = c_{14}(T)\, HW\, g_1(R_{JB})\, g_2(M_W)\, g_3(Dip) \tag{17}$$

Where *HW* set to 1.0 for sites affected by hanging wall.

4.6 Site response

Youngs [24] indicated that the soil amplification is a function of expected peak acceleration on rock. This approach allows a single regression between soil and rock attenuation. The linear and non-linear soil response is modeled by

$$f_8(V_{S30}, V_{lin}, PGA_{non-lin}, PGA_{rock}) = g_4(V_{S30}, V_{lin}) + g_5(PGA_{non-lin}, PGA_{rock}) \tag{18}$$

Based on this approach, the site amplification equation can be divided into two portion named linear and nonlinear terms.

4.6.1 Linear site response

The log of amplification can be modeled as a linear function of $\ln(V_{S30})$, consistent with the model developed by Boore et al. [25]. At short periods ($T \leq 0.5$sec), the scaling with $\ln(V_{S30})$ continues to higher V_{S30} values, but at long periods ($T \geq 0.75$sec), there is a break in the scaling with the amplification becoming independent of the V_{S30} above the break point. This break in the V_{S30} dependence indicates that for rock sites ($V_{S30} > 760m/s$) the V_{S30} is not strongly correlated with the deeper structure that affects the long period response. We did not solve for the site amplification terms in our analysis, but rather used a slight modification of the site amplification given by Choi and Stewart [19]. Choi and Stewart developed empirical amplification factors for NEHRP categories based on the V_{S30} and the PGA on rock. The equation and the coefficients of the equation are provided in each period for each NEHRP category. The linear site amplification equation is given by

$$g_4(V_{S30}, V_{lin}) = c_{15}(T)\ln\left(\frac{V_{S30}}{V_{lin}}\right) \tag{19}$$

Where $c_{15}(T)$ is a period dependent coefficient, and V_{lin} is the specified reference velocity and is a period-dependent. These coefficients were prescribed based on the work of Choi and Stewart [19]; they are empirically based, but were not determined by the regression analysis in our study.

4.6.2 Non-linear site response

The most direct approach would to estimate the non-linearity empirically as part of the regression analysis, but it can be difficult to extract the non-linearity since the vast majority of the data are in the linear range and non-linear site response can be laid by other terms in the ground motion model. We chose to use the results of the analytical site response model to constrain the non-linearity because the non-linearity from the analytical results is not correlated with other parameters and the analytical results provide better constraints on the non-linearity at high ground motion levels than the empirical data. In our model we use the PGA for $V_{S30} > 760m/s$ in place of the PGA_{rock} as the parameter describing the strength of the shaking. As the V_{S30} increases, the non-linearity will decrease until the amplification becomes linear. The nonlinear term is given by

$$g_5(PGA_{non-lin}, PGA_{rock}) = c_{16}(T)\ln\left(\frac{PGA_{non-lin}}{PGA_{rock}}\right) \tag{20}$$

Another form of the above formulation can be given by

$$g_5\left(PGA_{non-lin}, PGA_{rock}\right)=\begin{cases} c_{16}(T)\ln\left(\dfrac{PGA_{\min}}{0.1}\right) & PGA_{non-lin} < a_1 \\ c_{16}(T)\left[\ln\left(\dfrac{PGA_{\min}}{0.1}\right)+a\ln\left(\dfrac{PGA_{non-lin}}{a_1}\right)+b\left(\ln\left(\dfrac{PGA_{non-lin}}{a_1}\right)\right)^2\right] & a_1 \le PGA_{non-lin} \le a_2 \\ c_{16}(T)\ln\left(\dfrac{PGA_{non-lin}}{0.1}\right) & a_2 \le PGA_{non-lin} \end{cases} \quad (21)$$

Where $a_1(0.04g)$ and $a_2=(0.1g)$ are assigned to threshold levels for linear and nonlinear amplification, respectively, PGA_{min}=(0.06g) is a variable assigned to transition between linear and nonlinear behaviors, a and b are the coefficient to describe parabolic variation of $\ln\left(\frac{PGA_{non-lin}}{a_1}\right)$ form $\ln\left(\frac{PGA_{\min}}{0.1}\right)$ to $\ln\left(\frac{PGA_{non-lin}}{0.1}\right)$. $PGA_{non\text{-}lin}$ is the expected peak acceleration in g on rock as predicted by median attenuation relation for rock category ($V_{S30}=760m/s$). The period-dependent and V_{S30} dependent coefficients $c_{15}(T)$, $c_{16}(T)$, are prescribed based on a slight modification of the empirical analysis results presented by Choi and Stewart [19], where the modification was designed to smooth the predicted soil amplifications more effectively over amplitude and V_{S30}. As discussed above, the three equations for the nonlinear portion of the soil response are required for prevent the nonlinear amplification from increasing indefinitely as $PGA_{non\text{-}lin}$ decreases and to smooth the transition from amplification to no amplification. It is important to emphasize that the site response equations were prescribed is based on the work of Choi and Stewart, rather than determined by our regression. The reason for this is that we were concerned that the our database would be insufficient to simultaneously determine all coefficients for the nonlinear soil equations and the magnitude distance scaling, due to trade-offs that occur between parameters, particularly when soil nonlinearity is introduced. It is recognized that there are implicit trade-offs involved, and that a change in the prescribed soil response equations would lead to a change in the derived magnitude and distance scaling.

4.7 Basin response simulations

Based on the results from the primarily model analysis, we consider the soil depth effect to be significant. The SCEC 3-D basin response modeling group simulated the long period ground motions in the Los Angeles San Gabriel, and San Fernando basins in southern California region from nine different fault sources inside and outside of the basin [13, 14]. The results were summarized in terms of the amplification with respect to a hard rock site condition (V_S=3100(m/s)) as a function of the depth to a specified V_S isosurface. Day et al. [13] presented the results using the depths to V_S=1500(m/s) and $V_S=2500(m/s)$. In our model, we used a depth to V_S=1500(m/s) since it has a much better chance of being obtained for engineering projects.

From Day, the median 3-D basin amplification with respect to V_S=3100(m/s) was parameterized by the model of long period for deep sediments. We modified the amplification from the 3-D basin modeling to be consistent with our ground motion model. Do to the plentiful of the $Z_{1.5}$ values in our database; we decided to use this parameter in the regression analysis.

The functional form used to model sediment depth has two parts, a term to model 3-D basin effects for deep sediments in long periods and a term to model shallow-sediment effects for short and long periods. However we can scaling these two effects as a functions bellow

$$f_9(V_{S30}, Z_{1.5}) = g_6\left(V_{S30}, Z_{1.5}, \hat{Z}\right) + g_7(Z_D, Z_{1.5}) \tag{22}$$

Since V_{S30} is correlated with the $Z_{1.5}$, we combine these two estimates of the site amplification. The model for the long period site amplification should include both V_{S30} and $Z_{1.5}$, but it must account for the correlation of the two parameters. Parametric model for the shallow basin simulations can be equally well modeled by either a function of ln(V_{S30}) and a function of ln($Z_{1.5}$). The site response model response for shallow soil sites can be written as by

$$g_6\left(V_{S30}, Z_{1.5}, \hat{Z}\right) = c_{17}(T)\left(1/\hat{Z}\right)\ln\left(\frac{V_{S30}}{1500}\right)\ln(Z_{1.5}) \tag{23}$$

Where $\hat{Z}$ is the median $Z_{1.5}$ for the given V_{S30} and it should be constrained to model. 3-D basin amplification model was developed by Day et al. is for oscillator periods of 2.0 s and greater, but these authors developed relationships for their model coefficients which allowed us to extrapolate them to shorter periods. In order to remove any bias that this extrapolation might cause, we included an additional model coefficients to empirically adjust the theoretical model coefficient.

$$\begin{aligned} g_7(Z_{1.5}, Z_D) = {} & Z_D\, c_{18}(T) K_1 \left(1 - \exp\left(-(Z_{1.5} - 200)/300\right)\right) + \\ & Z_D\, c_{19}(T) K_2 \left(1 - \exp\left(-(Z_{1.5} - 200)/4000\right)\right) \end{aligned} \tag{24}$$

Where Z_D set to zero for shallow sediment depth and take 1.0 for deep sediment. This additional coefficient was found to increase at longer periods. The coefficients $c_{18}(T)$ and $c_{19}(T)$ are obtained unity in the regression analysis and constrained to unity at longer periods. Because the Day et al. model was applied only at large sediment depth, the second function (g_7) set to be zero if $Z_{1.5} \leq 200(m)$.

4.8 Standard error

Several recent attenuation studies have found that the standard error is dependent on the magnitude of the earthquake [3,6,7]. In this study both inter-event τ and intra event σ standard errors are allowed to be magnitude dependent and are modeled as linear magnitude dependence. The magnitude dependence of standard error is estimated using the random effects model, which avoids under estimating the standard error for large magnitude events due to the fewer number of events as compared to small and moderate magnitude events. The total standard error is the computed by adding the variance of the two error terms. The total standard errors was then smoothed and fit to the this bellow form

$$\sigma_{total}(M_W)=\begin{cases} c_{20}(T)+(c_{21}(T)-c_{20}(T))\,M_W & 5.0 \le M_W < 7.0 \\ c_{21}(T) & M_W \ge 7.0 \end{cases} \quad (25)$$

4.9 Regression analysis

It is not applied any weights during the regression analysis because of the relatively uniform distribution of recordings with respect to magnitude and distance (Figure 1). As in any independent regression analysis on individual spectral ordinates, there was a considerable amount of period-to-period variability in the regression coefficients.

They would lead to variability in the predicted acceleration response spectra, especially when extrapolated to small distances and large magnitudes. In order to reduce this variability, we did a limited amount of smoothing of the regression coefficients. The regression is computed using multiple steps. The multiple steps are used to constrain the resulting model to be smooth function of period for all magnitude, distance, mechanism and site condition.

Follow each step, the period dependence of the uncorrelated coefficients was smoothed using piecewise continuous linear fits on the log period axis. For highly correlated coefficients, one coefficient was smoothed and then the other coefficients were estimated again. Table 2 gives the coefficients for horizontal peak ground acceleration and acceleration response spectra and standard deviations of the equations.

5. Results of the Empirical Model

The resulting ground motion relations for selected response spectral ordinates are plotted in Figure 2. The rock site refer to site with average shear velocity is about V_{S30}=1130(*m/s*). In addition response spectra for soil site is shown in Figure 3. The soil site refers to site with average shear velocity about V_{S30}=270(*m/s*).

As it has shown in Figure 3 the amplitude, in soil site (soft clays) is grater than rock site for PGA and PSA at short periods and indicates the soil site may increase the amplitude of strong ground motions in short to median periods. Predicted response spectra showing the effect of magnitude are plotted in Figure 4.

In generally the predicted response spectra grow with magnitude. In the site condition, we have large amplitude in median periods when magnitude is increase. The effects of style of faulting mechanism and local site condition are plotted in Figure 5. We expected to have increase in ground motion in reverse faulting mechanism respected to strike-slip and normal faulting. Predicted response spectra plotted for reverse event show more amplitude in median and long periods compared to strike-slip and normal events.

Spectral acceleration based on site condition that is shown in Figure 5 indicates that the behavior of spectral acceleration with respected to site conditions is significantly different. The amplitudes for soft soil and soft rock are somewhat higher at short periods and the amplitudes for firm rock and hard rock are significantly lower at long periods for the specific values of magnitude (M_W=7.0) and distance (R_{rup}=10*km*) used in the evaluation.

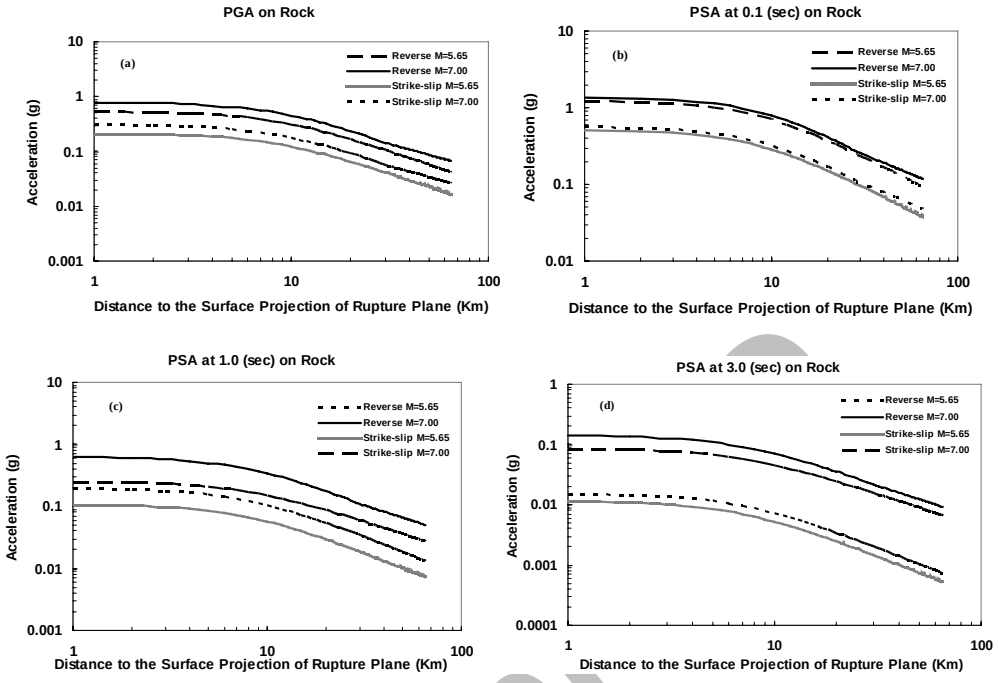

Figure 2. Ground-motion relations from this study for reverse and strike-slip faulting for the rock site (V_{S30}=1130 m/s): (a) Corrected PGA, (b) PSA at 0.1 sec, (c) PSA at 1.0 sec, and (d) PSA at 3.0 sec

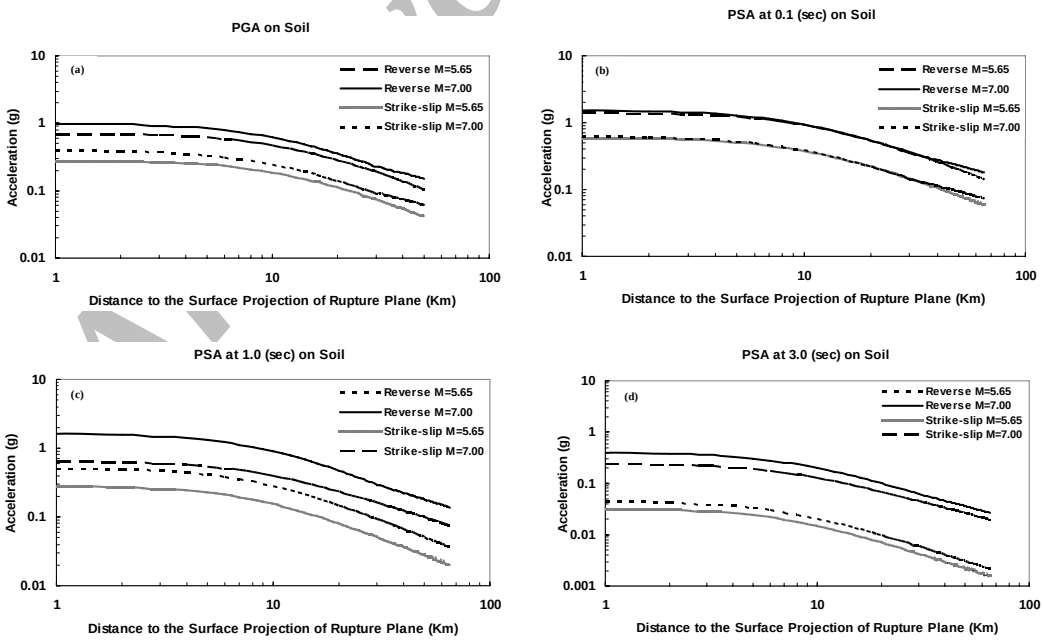

Figure 3. Ground-motion relations from this study for reverse and strike-slip faulting for the soil site (V_{S30}=270 m/s): (a) Corrected PGA, (b) PSA at 0.1 sec, (c) PSA at 1.0 sec, and (d) PSA at 3.0 sec

Table 2. Coefficients and Statistical Parameters from the Regression Analysis of PGA and PSA

T (sec)	C_1	C_2	C_7	C_8	C_9	C_{10}	C_{11}	C_{12}	C_{13}	C_{14}	C_{15}	C_{17}	C_{18}	C_{19}	C_{20}	C_{21}	K_1	K_2	V_{lin}
0	1.81	-1.18	8.647	-0.028	-0.176	-0.266	-0.476	0.52	-0.32	0.4	-0.36	0	0	0	0.496	0.427	2.260	1.04	760
0.025	2.161	-1.184	8.443	-0.024	-0.276	-0.351	-0.592	0.52	-0.319	0.448	-0.335	0	0	0	0.498	0.432	2.255	1.047	407
0.04	2.54	-1.203	8.427	-0.018	-0.376	-0.477	-0.737	0.52	-0.318	0.471	z-0.31	0	0	0	0.503	0.443	2.252	1.05	233
0.05	2.715	-1.218	8.417	-0.012	-0.442	-0.477	-0.737	0.52	-0.317	0.471	-0.29	0	0	0	0.504	0.450	2.25	1.053	192
0.075	2.82	-1.221	8.39	0.002	-0.442	-0.477	-0.737	0.519	-0.315	0.418	-0.23	0	0	0	0.508	0.451	2.245	1.06	196
0.1	2.734	-1.182	8.364	0.01	-0.375	-0.436	-0.71	0.519	-0.313	0.351	-0.25	0	0	0	0.520	0.452	2.24	1.066	257
0.12	2.703	-1.158	8.342	0.005	-0.319	-0.403	-0.684	0.519	-0.311	0.351	-0.26	0	0	0	0.509	0.452	2.236	1.071	299
0.15	2.626	-1.125	8.311	-0.004	-0.234	-0.353	-0.644	0.519	-0.309	0.351	-0.28	0	0	0	0.458	0.453	2.23	1.079	357
0.2	2.514	-1.1	8.258	-0.024	-0.149	-0.27	-0.577	0.518	-0.305	0.35	-0.31	0	0	0	0.557	0.476	2.22	1.092	453
0.3	2.404	-1.1	8.152	-0.051	-0.149	-0.237	-0.444	0.517	-0.291	0.349	-0.44	0	0	0	0.552	0.489	2.201	1.118	532
0.4	2.295	-1.1	8.046	-0.07	-0.149	-0.237	-0.311	0.516	-0.277	0.348	-0.5	-0.15	-0.32	0	0.5535	0.489	2.181	1.144	535
0.5	2.208	-1.107	8.005	-0.088	-0.037	-0.186	-0.178	0.515	-0.263	0.347	-0.6	-0.15	0.153	0.105	0.578	0.489	2.161	1.171	535
0.75	2.076	-1.148	7.901	-0.129	0.15	0.1357	-0.112	0.512	-0.229	0.345	-0.69	-0.15	0.153	0.3	0.584	0.489	2.112	1.236	535
1	1.945	-1.185	7.798	-0.175	0.15	0.2	-0.112	0.509	-0.143	0.327	-0.7	-0.15	0.153	0.307	0.586	0.489	2.062	1.301	535
1.5	1.767	-1.222	7.591	-0.245	0.15	0.2	-0.112	0.504	0	0.292	-0.72	0.317	0.153	0.456	0.592	0.489	1.963	1.432	535
2	1.544	-1.259	7.385	-0.295	0.15	0.2	-0.112	0.479	0	0.257	-0.73	0.317	0.258	0.806	0.610	0.489	1.864	1.562	535
2.5	1.462	-1.289	7.178	-0.336	0.15	0.2	-0.112	0.424	0	0.222	-0.735	0.405	0.258	0.806	0.623	0.489	1.765	1.693	535
3	1.318	-1.289	6.971	-0.381	0.15	0.2	-0.112	0.368	0	0.188	-0.74	0.405	0.258	0.778	0.635	0.489	1.666	1.823	535
3.5	1.208	-1.289	6.765	-0.416	0.15	0.2	-0.112	0.313	0	0.154	-0.745	0.405	0.258	0.706	0.646	0.489	1.567	1.954	535
4	1.063	-1.28	6.558	-0.443	0.15	0.2	-0.112	0.258	0	0.121	-0.75	0.405	0.258	0.635	0.662	0.489	1.468	2.084	535
4.6	0.824	-1.265	6.31	-0.466	0.15	0.2	-0.112	0.169	0	0.08	-0.75	0.672	0	0.55	0.668	0.489	1.349	2.241	535
5	0.682	-1.256	6.145	-0.482	0.15	0.2	-0.112	0.125	0	0.053	-0.75	0.672	0	0.493	0.671	0.490	1.27	2.345	535
6	0.392	-1.232	5.731	-0.52	0.15	0.2	-0.112	0	0	0	-0.7268	0.085	0	0.351	0.673	0.492	1.072	2.606	535
7	0.158	-1.209	5.318	-0.559	0.15	0.2	-0.112	0	0	0	-0.7036	0.085	0	0.28	0.673	0.493	0.874	2.867	535
8	-0.065	-1.185	4.905	-0.598	0.15	0.2	-0.112	0	0	0	-0.6836	0.085	0	0.28	0.674	0.495	0.676	3.128	535
9	-0.261	-1.162	4.491	-0.637	0.15	0.2	-0.112	0	0	0	-0.6668	0.085	0	0.28	0.674	0.496	0.478	3.389	535
10	-0.434	-1.138	4.078	-0.676	0.15	0.2	-0.112	0	0	0	-0.65	0.085	0	0.28	0.683	0.496	0.28	3.65	535

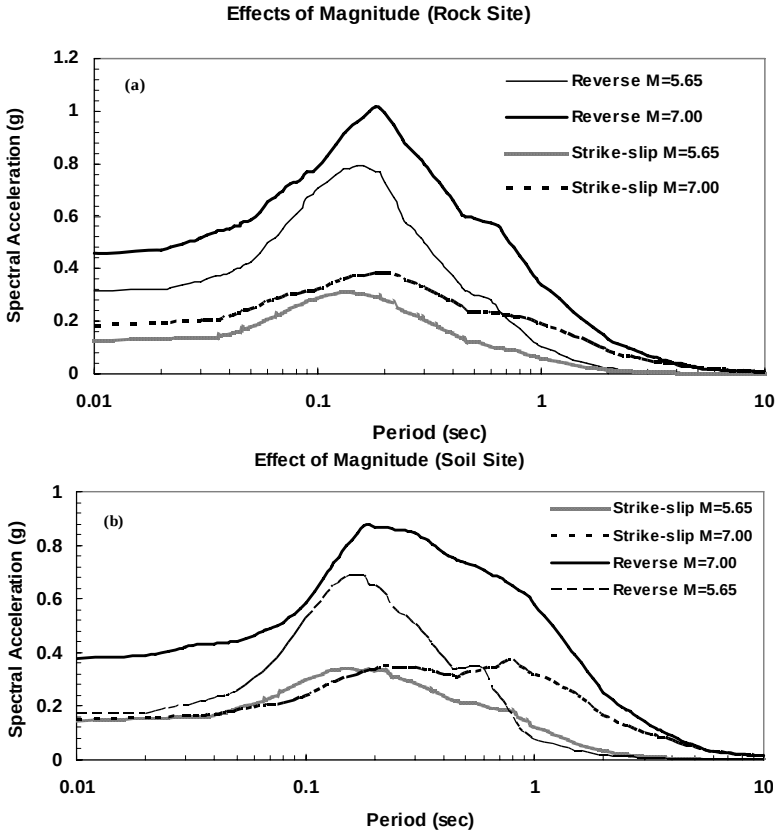

Figure 4. PSA (5% damping) predicted from the ground-motion relations developed in this study showing the effects of (a) magnitude for the rock site V_{S30}=1130 (m/s), (b) magnitude for the soil site V_{S30}=270 (m/s). It should be noted, the spectra are evaluated for M_W=7.0 and M_W=5.65 in distance R_{rup} = 10 (km) for reverse and strike-slip faulting

Thrust faulting events have somewhat higher amplitudes at some periods compared to strike-slip and normal faulting events. There is a greater opportunity for sites to be located over the hanging wall of reverse and thrust faults than strike-slip and normal faults, which increases their likelihood for higher ground motion at close distances.

The regression models for the horizontal components of PGA and PSA were demonstrated using an analysis of residuals. For purposes of this analysis, we defined an extra-event residual as

$$\varepsilon_{ij} = \left(\ln Y_{ij} - \ln \overline{Y}_{ij}\right) / \sigma_{total} \tag{26}$$

Where ln Y_{ij} is the natural logarithm of the ij th observed value of Y, ln $\overline{Y}_{ij}$ is the natural logarithm of the ij th predicted value of Y, and σ_{total} is the standard deviation of the natural logarithm of PGA or PSA.

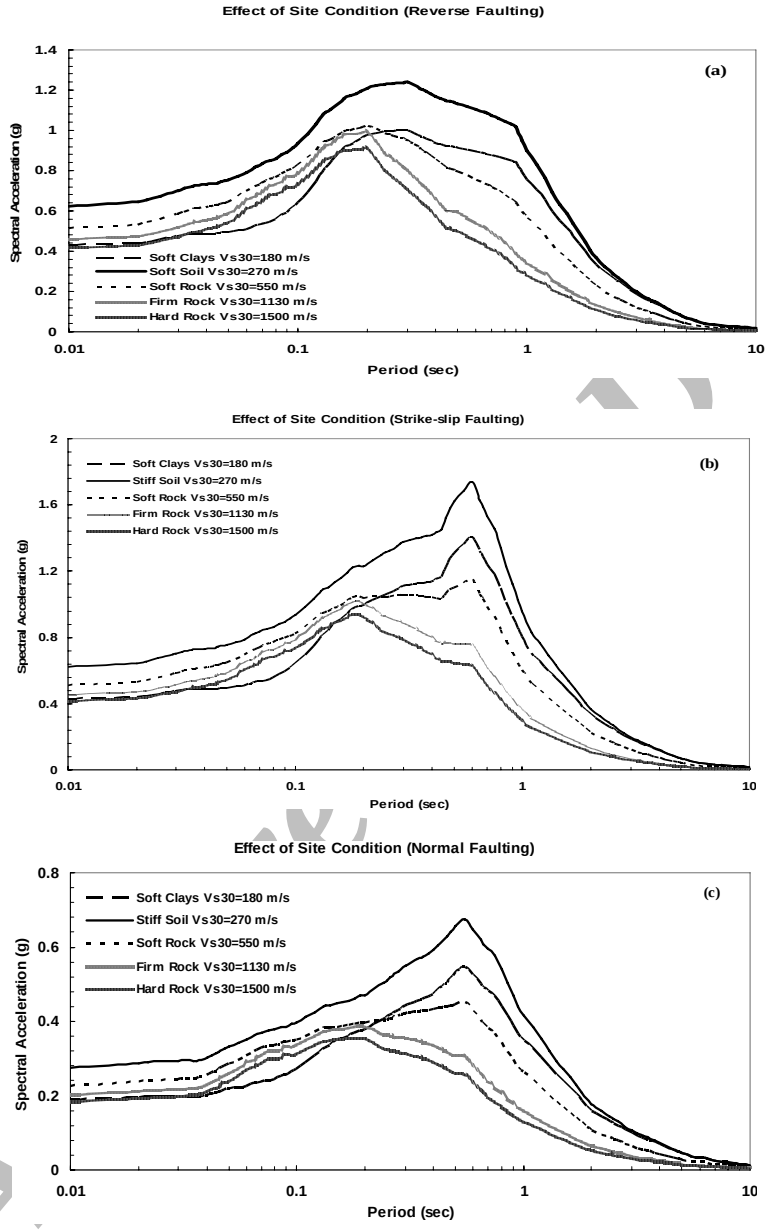

Figure 5. PSA (5% damping) predicted from the ground-motion relations developed in this study showing the effects of faulting mechanism (a) reverse, (b) strike-slip and (c) normal for different local soil conditions for the horizontal component of ground motion, the spectra are evaluated for M_W=7.0, R_{rup}=10 (km). The reverse-faulting category has amplitudes that are approximately more than the strike-slip and normal faulting categories, although this difference varies with period

The intra-event residuals were normalized by σ_{total} in order to better imagine the relative differences in the scatter in the intra-event residuals among the different strong motion

parameters. For the model to be unbiased, the intra-event residuals should have zero mean and be un-correlated with respect to the parameters in the regression model. The intra-event residual plots for the average horizontal component of ground motion as a function of magnitude and distance for selected response spectral ordinates are shown in Figure 6 and Figure 7, respectively. These Figures indicate that the regression models are unbiased with respect to these two parameters.

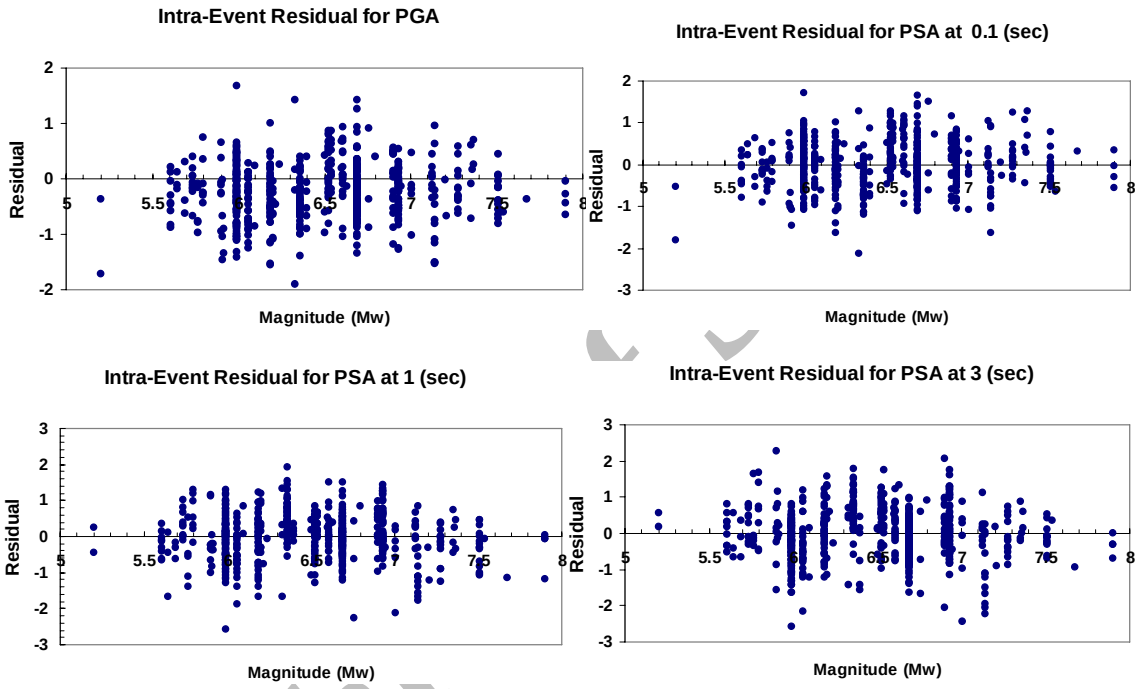

Figure 6. Ground motion intra-event residuals as a function of magnitude for the regression analysis of the average horizontal component of ground motion: (a) PGA, (b) PSA at 0.1 sec, (c) PSA at 1.0 sec, and (d) PSA at 3.0 sec

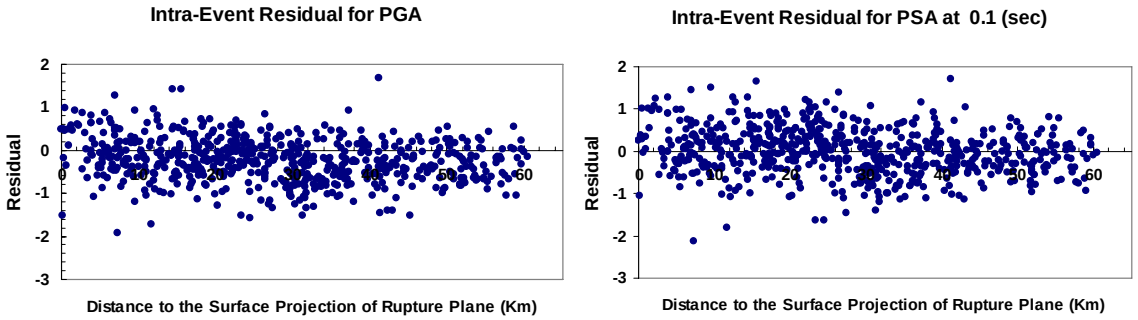

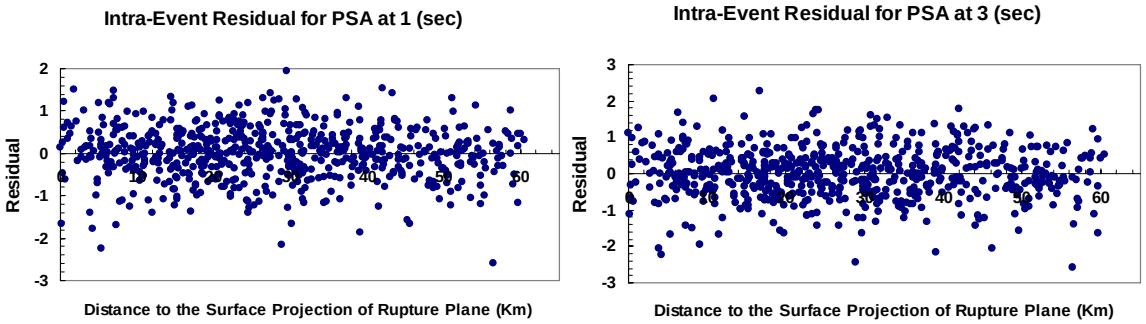

Figure 7. Ground motion extra-event residuals as a function of distance for the regression analysis of the average horizontal component of ground motion: (a) PGA , (b) PSA at 0.1 sec, (c) PSA at 1.0 sec, and (d) PSA at 3.0 sec

Other plots show similarly unbiased results for faulting mechanism, site conditions and other parameters.

In Figure 8 we presented the results of using the depths to V_S=1500 (*m/s*) (it has a much better chance of being obtained for engineering projects) for different sediment depth. As it is shown in Figure 8 the amplification of spectra will increase when sediment depth growth. It is verified with the work of SCEC group (Day et al.). This amplification in more important for deep sediments in long period ground motions.

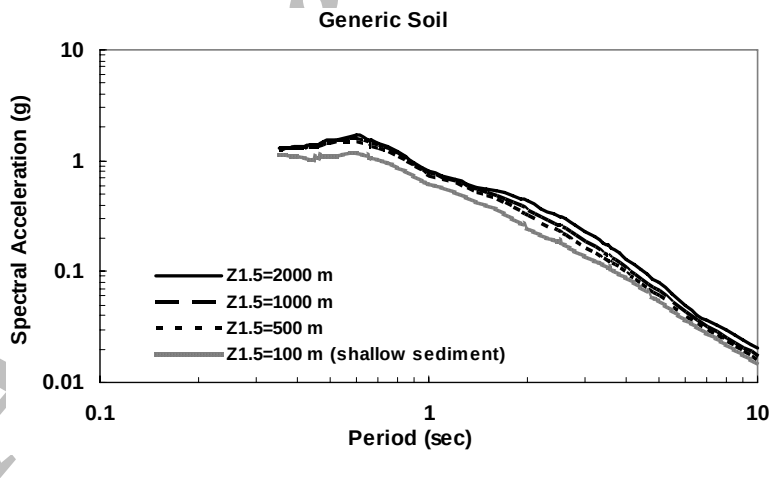

Figure 8. Summary of results from the basin response simulations based on depth to the V_S=1.5 (km/s) isosurface from our study for deferent sediment depth. As it shown, the amplitude of PSA increase respected to base sediment depth in long periods ground motions

6. Comparison with Previous Studies

We compared our new ground motion relations with six ground motion relations that are

widely used to estimate horizontal response spectra for seismological and engineering analyses in non-extensional regions [2,3,4,6,7,15].

All the relations address the average horizontal component for both soil and rock. These relations represent a seismically active, shallow-crustal tectonic environment, consistent with our study. They all define the faulting mechanism to strike-slip and reverse categories, where our study includes both reverse and strike-slip faulting as defined normal faulting. They all use different definitions for local site conditions. Sadigh et al. [7] claimed that their relations for rock include sites with no more than 1 (m) of soil overlying rock; however, Youngs (personal comment, 2002) has suggested that this is not strictly true and that the rock sites include thicker layers of soil, possibly up to 20 (m). The Sadigh et al. [7] relation for soil includes sites with greater than 20 (m) of soil overlying rock. The Abrahamson and Silva [6] relation uses the soil definition of Sadigh et al. [7] and defines rock as a deposit with less than 20 (m) of soil overlying rock. It differentiates between these two categories using an amplitude-dependent site factor. The Boore et al. [15] relation accounts for site effects using the velocity parameter, V_{S30}. According to Boore and Joyner [25], sites classified as generic soil, as defined by Boore et al. [15], are consistent with a 30(m) velocity of about 310(m/sec), and sites classified as generic rock are consistent with a 30(m) velocity of about 620(m/sec). The Campbell [2] relation classifies sites as generic soil, soft rock, or hard rock. Campbell and Bozorgnia [3] presents a more thorough summary of all four of these ground motion relations and suggests adjustments that make them more consistent with the definition of generic soil and generic rock given previously. For the evaluation given here, we did not make any adjustments to be consistent with current engineering practice. Figure 9 and Figure 10 compare the predicted median spectral acceleration from the six selected ground motion relations with that predicted from our ground motion relations for a site located 10 (km) from a reverse earthquake of M_W=7.0. This distance corresponds to R_{JB}=R_{rup}=10(km) and R_{seis}=10.4(km), assuming the fault ruptures to the surface and that the depth to seismogenic rupture is 3 (km) (Abrahamson and Shedlock [26], Campbell and Bozorgnia [3]). The R_{seis} is defined as the shortest distance between the recording site and the zone of the seismogenic energy release on the causative fault (referred to here as the distance to seismogenic rupture) used by Campbell and Bozorgnia [3]. Comparisons are shown for the two most common site conditions used in engineering analysis, namely, generic soil and generic rock. Our ground motion relation was evaluated for generic soil by setting V_{S30}=310(m/s) and for generic rock by setting V_{S30}=620(m/s). These values represent the approximate proportion of recordings in our database that comprise each of these categories. The comparisons in Figure 9 and Figure 10 shows that our relations predict spectral accelerations are generally similar to those of the other six ground motion relations when evaluated for generic soil and generic rock. Our ground motion periodic relatively more amplitudes at short and median periods. It was expected according to our data set for soil categories. This is especially true for stiff soil, which comprises only about 25% of the generic soil category but behaves similarly to soft rock, and for firm rock, which comprises 50% of the generic rock category but behaves significantly different from soft rock, especially at long periods. Our ground motion relations prediction relatively has same amplitudes at short periods for the horizontal component on generic rock, consistent with that of Boore et al. [15]. It is interesting to note

that the Boore et al. [15] relation is the only one that is specifically evaluated for V_{S30}=620(*m/s*), the real definition of generic rock. Because of the relatively large differences in ground motion for the site categories defined in our study, the comparison in Figure 9 and Figure 10 would not be so favorable for some of our other site conditions. Ambraseys and Douglas [4] suggesting to consider peak ground motion on generic rock and soiling 0.517 g and 0.546g, respectively.

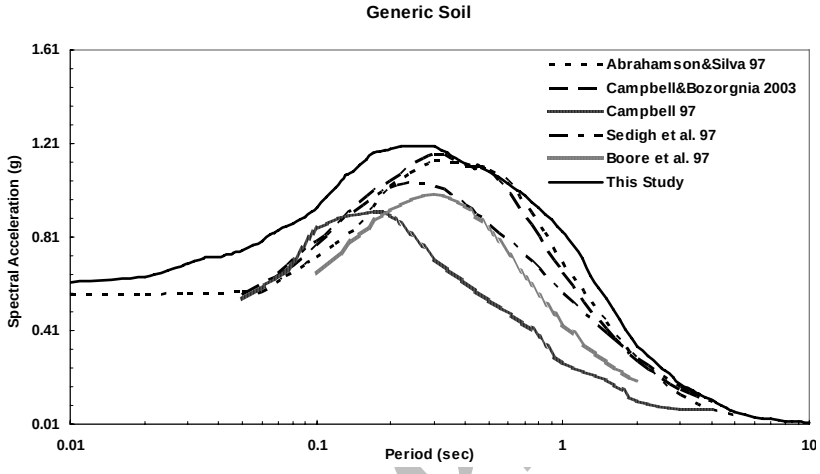

Figure 9. Comparison of predicted PSA (5% damping) for generic soil from ground-motion relation in this study and five ground-motion relations widely used in seismology and engineering. Generic soil is defined in the text but generally represent site with V_{S30}=310 (m/s). The spectra are evaluated for M_W= 7.0, R_{JB}=R_{rup}=10 (km), R_{seis}= 10.4 (km)

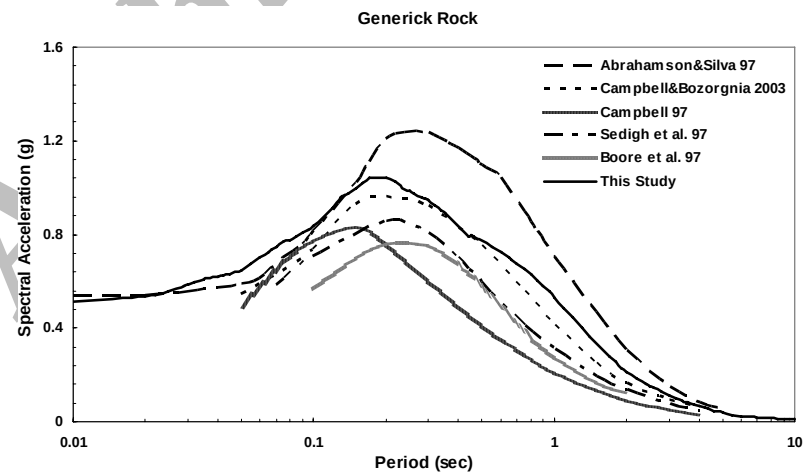

Figure 10. Comparison of predicted PSA (5% damping) for generic rock from ground-motion relation in this study and five ground-motion relations widely used in seismology and engineering. Generic rock is defined in the text but generally represent site with V_{S30}=620 (m/s). The spectra are evaluated for M_W= 7.0, R_{JB}=R_{rup}=10 (km), R_{seis}= 10.4 (km)

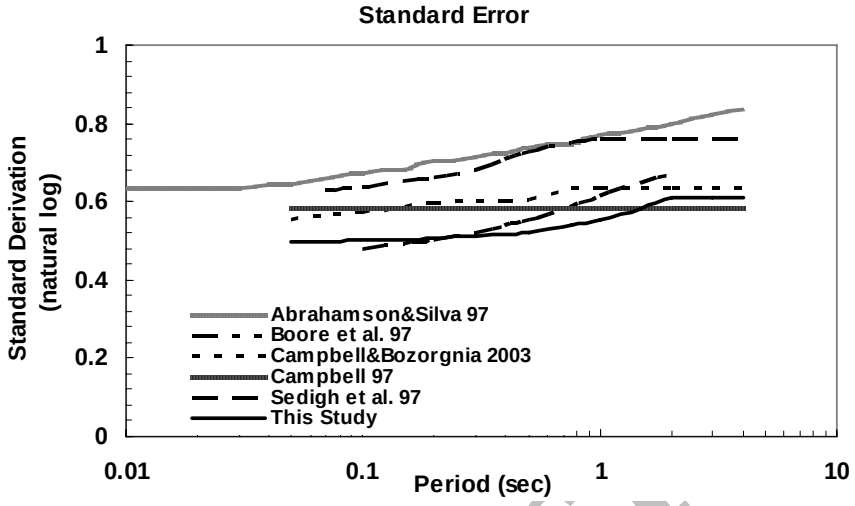

Figure 11. Comparison of predicted standard deviations of spectral acceleration ($\sigma_{\ln Y}$) from this study and five ground-motion relations widely used in seismology and engineering. The standard deviations are evaluated for M_W= 5.5

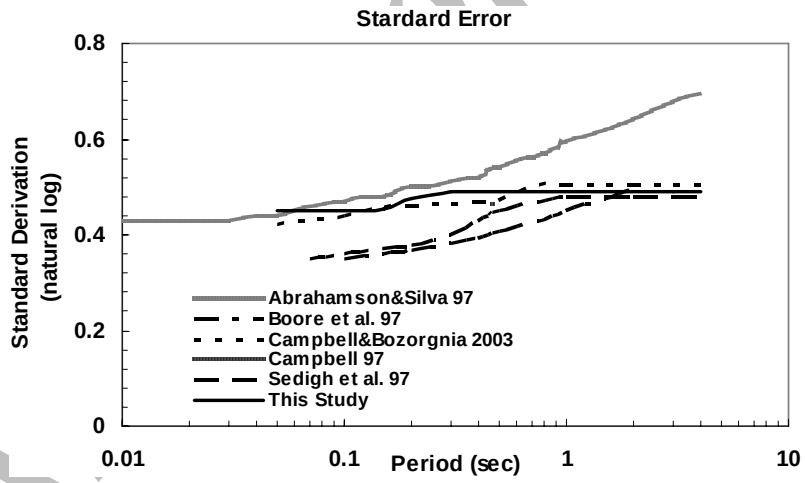

Figure 12. Comparison of predicted standard deviations of spectral acceleration ($\sigma_{\ln Y}$) from this study and five ground- motion relations widely used in seismology and engineering. The standard deviations are evaluated for M_W= 7.5

Only Boore et al. [15] addressed these differences by virtue of their site parameter, V_{S30}, but they did not incorporate nonlinear site effects. Figure 11 and Figure 12 shows a comparison of the standard deviations (natural log) predicted from the ground motion relations evaluated. The standard deviation is important because it contributes significantly to deterministic estimates of ground motion that are defined by the median plus one standard deviation and to probabilistic estimates of ground motion, especially at long return periods, where $\sigma_{\ln Y}$ can increase the

predicted ground motion, depending on its value. Figure 11 and 12 indicates that our horizontal standard deviations are among the lowest. Note that the horizontal standard deviations of Boore et al. [15] are independent of magnitude and plot among those for M_W=5.5 and M_W=7.5 in Figure 11 and Figure 12.

Figures 13 and 14 compare the attenuation characteristics of PGA predicted by the ground motion relations evaluated in for a suite of sites located on the hanging wall of a 45º dipping thrust fault. The event is intentionally large (M_W=7.5), and PGA is plotted on a linear scale to accentuate the hanging wall effects. All of the relations are plotted versus the distance measure, R_{rup}, for purposes of comparison. Only our relation, Abrahamson and Silva [6] relation and Campbell and Bozorgnia [3] relation explicitly include hanging wall effects.

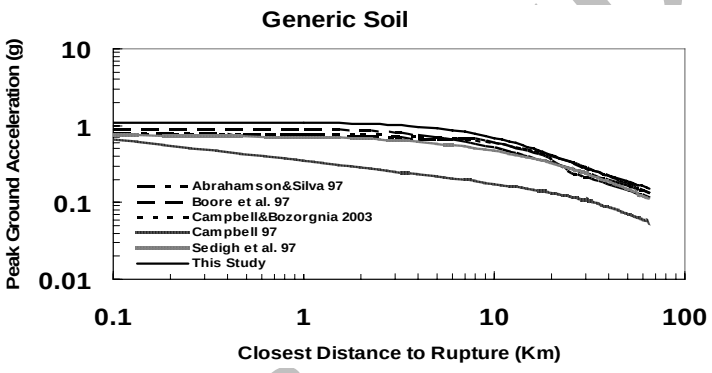

Figure 13. Comparison of predicted PGA for generic soil on the hanging wall between this study and four horizontal ground-motion relations widely used in seismology and engineering. Generic soil in is defined the text but generally represent sites with V_{S30}=310 (m/s). The relations are evaluated for M_W =7.5 and for a reverse or thrust fault dipping at 45 degree

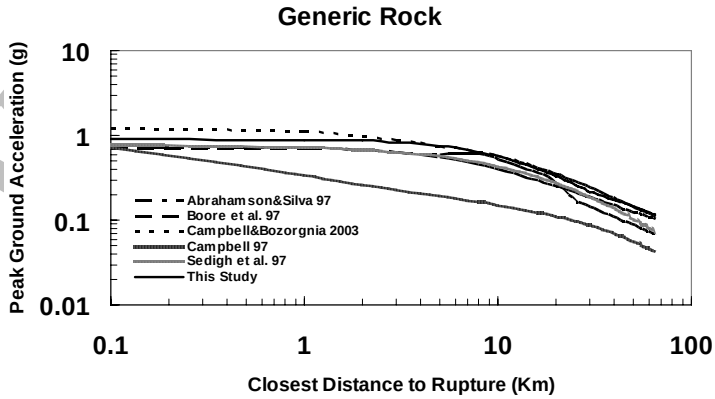

Figure 14. Comparison of predicted PGA for generic rock on the hanging wall between this study and four horizontal ground-motion relations widely used in seismology and engineering. Generic rock is defined in the text but generally represent sites with V_{S30}=620 (m/s). The relations are evaluated for M_W =7.5 and for a reverse or thrust fault dipping at 45 degree

The Boore et al. [15] relation inherently includes hanging wall effects by virtue of its distance measure R_{JB}. The value of PGA predicted by the Campbell [2] relation decreases at very small values of R_{rup} once its distance measure, R_{seis}, begins to increase past the point at which the top of the 3(km) seismogenic depth on the fault is reached. Our relation would do the same, except that the hanging wall effects keep it approximately constant at these small distances.

Our generic rock results are similar to those of Campbell and Bozorgnia [3], where our predictions remain constant and theirs begin to increase. Although the Boore et al. [15] predictions show similar behavior, the constant part of the curve occurs at a much smaller value of PGA. Our generic soil results show a small effect of the hanging wall because of the site category referred to stiff soil (remember that there are no additional hanging-wall effects for firm soil or soft clays). The Abrahamson and Silva [6] relation shows more subdued hanging wall effects because of nonlinear soil behavior. In the case of generic soil, our relation and Boore et al. [15] relation predicts much higher PGA, possibly due to a lack of nonlinear effects.

7. Conclusions

We consider the ground motion relations developed in this study to be valid for estimating PGA and 5% damped PSA for earthquakes of $M_W \geq 5.2$ and distances of $R_{rup} \leq 60(km)$ for shallow crustal earthquakes in the similar seismically active tectonic regimes worldwide. The relations can be extrapolated to a distance of 100(km) without serious compromise, but like all of the empirical models evaluated in this article, they should not be used beyond this distance without carefully considering the possible engineering consequences. For example, like many of the other relations, our relations over predict ground motion beyond 100 (km), therefore provide a conservative engineering estimate of ground motion at these distances. We consider our ground motion relations to supersede previous relations [2, 3, 4, 6, 7, 15], except when sediment depth and nonlinear soil behavior needs to be evaluated, which are included in our relation. Although there was a limited attempt to smooth the trends in the regression coefficients of our ground motion relations, the resulting spectra still exhibit some period-to-period variability. Therefore, we recommend that the ground motion predicted from these relations be averaged with that from other credible ground motion relations when calculating engineering estimates of ground motion, consistent with the common engineering practice of incorporating epistemic variability. Since the range of for firm rock has a mean that is higher than that corresponding to the NEHRP BC boundary (760 (m/sec)) used to define the reference site condition in the USGS seismic hazard maps, we recommend that horizontal ground motion for this latter site condition be calculated from our generic rock prediction. It is important to recognize that this study was intended to be a development of the ground motion relations, with the explicit purpose of providing engineers and seismologists with a mutually consistent set of near-source ground motion relations to use in seismic hazard analysis. Being this development, the study explicitly addresses such topics as sediment depth and the use of the 30(m) velocity or related NEHRP site classes. However, we refine some of the parameters previously used, by including

hanging wall effects, dividing faulting mechanism to three main categories (reverse, strike-slip and normal faulting), sediment depth effect, depth-to-top of the rupture effects and finally nonlinear soil response in our model. Based on the empirical analysis performed in this study, we found specific observations and conclusions. We found the common practice of using generic soil and generic rock to define local site conditions to be too simplistic.

We found the seismic behavior of stiff soil, the stiffer component of generic soil, to be closer to that of soft rock than to that of firm soil, the softer component of generic soil. Furthermore, we found the seismic behavior of firm rock, the harder component of generic rock, to be significantly different from that of soft rock, the softer component of generic rock. These observations are consistent with the approximate range of 30(m) velocity for these site categories given in Table 3. By considering five site categories, we found apparent strong nonlinear behavior only for the short period, horizontal component of ground motion on stiff soil, probably because of its lower stiffness and its greater likelihood of being saturated. Although not addressed in our study, other studies have also shown soft soil to have significant nonlinear site effects. We found the greatest differences in median predicted ground motion among the five site categories defined in this study. At long periods, firm rock has significantly lower amplitudes due to an absence of sediment amplification, and at short periods, stiff soil has relatively low amplitudes at large magnitudes and short distances due to nonlinear site effects. We found differences in median-predicted spectral acceleration among strike-slip, reverse, and normal faulting earthquakes to be consistent with differences in dynamic stress drop. These differences were found to become negligible at periods of 2.0(sec) and greater, where dynamic stress drop is expected to have little impact on the amplitude of strong ground motion. This result could help to explain the large ground motion observed during several recent blind-thrust earthquakes, which have been shown from independent seismological studies to have relatively large dynamic stress drop. There are, however, more opportunities for hanging wall effects on the shallower dipping thrust faults, which will lead to a greater number of sites with relatively high ground motion as compared to the other faulting mechanism.

Table 3. Site categories in *NEHRP Provisions*

NEHRP Category	**Description**	**Mean Shear Wave Velocity to 30 m**
A	Hard rock	> 1500 m/s
B	Firm to hard rock	760-1500 m/s
C	Dense soil, soft rock	360-760 m/s
D	Stiff soil	180-360 m/s
E	Soft clays	< 180 m/s
F	Special study soils, e.g., liquefiable soils, sensitive clays, organic soils, soft clays >36 m thick	

Additional study is needed to determine exactly what additional earthquake source characteristics can be expected to result in higher ground motions from thrust (especially blind-thrust) faults. We found that the modified model for hanging wall effects presented in our study could be used for ground motion relations. However, we restricted the definition of the hanging wall to be that part of the crust over the rupture plane, with a 30(km) margin defined in terms of the distance measure, R_{JB}, to allow for a smooth transition from hanging wall to no hanging wall effects. We also found that hanging wall effects were less significant for firm soil sites, whose ground motion amplitudes at short distances and large magnitudes had apparently already reached the limit allowed by nonlinear site effects. Based on an analysis of residuals, we found sediment depth (depth to basement rock) to have a significant effect on the amplitude of ground motion, especially at long periods $T \geq 2$(sec). Sediment depth was included as a parameter because its effect, especially its correlation with other parameters in the model is understood. Furthermore, its exclusion is a practical limitation, since it is typically used in engineering analyses. It is not included in any other previous ground motion relation used in engineering or seismology. An analysis of residuals determined that the residual of the PGA and response spectral predicted from our ground motion relations were unbiased with respect to magnitude, distance, faulting mechanism, source to top and site conditions. This indicates that these relations are mutually consistent and, therefore, can be used to develop engineering estimates of horizontal ground motion.

References

1. Campbell KW, Bozorgnia Y. Near-source attenuation of peak horizontal acceleration from worldwide accelerograms recorded from 1957 to 1993. Processing of 5th U.S. National Conference on Earthquake Engineering, Earthquake Engineering Research Institute, Oakland, California, **3**(1994) 283-92.
2. Campbell KW. Empirical near-source attenuation relationships for horizontal and vertical components of peak ground acceleration, peak ground velocity, and pseudo-absolute acceleration response spectra. *Seismological Research Letters*, **68**(1997) 154–79.
3. Campbell KW, Bozorgnia Y. Updated near-source ground-motion (attenuation) relations for the horizontal and vertical components of peak ground acceleration and acceleration response spectra, *Bulletin of Seismological Society of America*, **93**(2003) 314-31.
4. Ambraseys NN, Douglas J. Near-field horizontal and vertical earthquake ground motions. *Soil dynamic and Earthquake Engineering*, **23**(2003) 1-18.
5. Joyner W.B, Boore DM. Peak horizontal acceleration and velocity from strong-motion records including records from the 1979 Imperial Valley California earthquake. *Bulletin of Seismological Society of America,* **71**(1981) 2011–38.
6. Abrahamson NA, Silva WJ. Empirical response spectral attenuation relations for shallow crustal earthquakes, Seismological Research Letters, **68**(1997) 94–127.
7. Sadigh K, Chang CY, Egan JA, Makdisi F, Youngs RR. Attenuation relationships for shallow crustal earthquakes based on California strong motion data, *Seismological Research Letters,* **68**(1997) 180–89.

8. Spudich P, Joyner WB, Lindh AG, Boore DM, Margaris BM, Fletcher JB. SEA99, A revised ground motion prediction relation for use in extensional tectonic regimes, *Bulletin of Seismological Society of America,* **89**(1999) 1156–70.
9. Atkinson GM, Boore DM. Evaluation of models for earthquake source spectra in eastern North America, Bulletin of Seismological Society of America, **88**(1998) 917–34.
10. Campbell KW. Empirical prediction of near-source ground motion for the Diablo Canyon Power Plant Site, San Luis Obispo County, California. *U.S. Geological Surveying Open-File Report,* 1989, pp. 89–484.
11. Lee Y, Anderson JG. Potential for improving ground motion relations in southern California by incorporating various site parameters. *Bulletin of Seismological Society of America*, **90**(2000) S170–86.
12. Joyner WB. Strong motion from surface waves in deep sedimentary basins. *Bulletin of Seismological Society of America,* **90**(2000) S95–112.
13. Day SM, Bielak J, Dreger D, Graves R, Larsen S, Olsen K, Pitarka A. 3D ground motion simulations in Basins, Final report prepared for the Pacific Earthquake Engineering Research Center, Project 1A03, 2005.
14. Day SM. Model of 3-D basin amplification factor relative to $Z_{1.0}$, Personal communication, 2005.
15. Boore DM, Joyner WB, Fumal TE. Equations for estimating horizontal response spectra and peak acceleration from western North American earthquakes: a summary of recent work, *Seismological Research Letters*, **68**(1997) 128–53.
16. Wills CJ, Silva WJ, Shear-wave velocity characteristics of geologic units in California, *Earthquake Spectra,* **14**(1998) 533–56.
17. Wills CJ, Petersen M, Bryant WA, Reichle M, Saucedo GJ, Tan S, Taylor G, Treiman J. A site-conditions map for California based on geology and shear-wave velocity, *Bulletin of Seismological Society of America*, **90**(2000) S187–208.
18. Park S, Elrick S. Predictions of shear-wave velocities in southern California using surface geology, *Bulletin of Seismological Society of America*, **88**(1998) 677-85.
19. Choi Y, Stewart JP. Nonlinear site amplification as function of 30 m shear-wave velocity, *Earthquake Spectra*, **21**(2005) 1-30.
20. Idriss IM. Selection of earthquake ground motions at rock sites. Report prepared for the Structures Division, Building and fire Research Labratury, NIST, 1991.
21. Somerville PG, Pitarka A. Differences in earthquake source and ground motion characteristics between surface and buried earthquakes. *Processing of 8th National Conference on Earthquake Engineering*, Paper No. 977, 2006.
22. Abrahamson NA, Somerville PG. Effects of the hanging wall and footwall on the ground motions recorded during the Northridge earthquake, *Bulletin of Seismological Society of America*, **86**(1996) S93-9.
23. Collins N, Graves R, Somerville PG. Revised analysis of 1D rock simulations for the NGA-E project, Final report prepared for the Pacific Earthquake Engineering Research Center, 2006.
24. Youngs RR. Soil amplification and vertical to horizontal ratios for analysis of strong motion data from active tectonic region, Appendix 2C in Guidelines for Determing Design Basis Ground Motions: appendices for ground motion estimation, TR-102293, 1993.

25. Boore DM, Joyner WB. Site amplification for generic rock sites, *Bulletin of Seismological Society of America,* **87**(1997) 327–41.
26. Abrahamson NA, Shedlock KM. Overview, *Seismological Research Letters,* **68**(1997) 9-23.